Recommended data for capture cross sections in B^{5+} + H collisions.

L. F. Errea[1], F. Guzmán[1,2], Clara Illescas[1], L. Méndez[1], B. Pons[3], A. Riera[1] and J. Suárez[1]

[1] Laboratorio Asociado al CIEMAT de Física Atómica y Molecular en Plasmas de Fusión, Departamento de Química C-IX, Universidad Autónoma, 28049 Madrid, Spain

[2] Laboratorio Nacional de Fusión por Confinamiento Magnético, CIEMAT, 28040 Madrid, Spain

[3] Centre Lasers Intenses et Applications, UMR 5107 du CNRS, Université de Bordeaux-I, 351 Cours de la Libération, 33405 Talence, France

Abstract. Recommended values for state selective capture cross sections are presented for the collision B^{5+} + H(1s) in the energy range from 0.05 keV/amu to 1000 keV/amu. Special attention is focused on capture processes to $n = 7$ states of B^{4+}, which play important role in spectral diagnostics in fusion plasmas. In order to completely cover the intermediate impact energy domain, quantal, semi-classical and classical treatments have been employed for low, low-intermediate and intermediate-high energies, respectively. We also give some guidelines about the domain of accuracy of the methodologies employed. Additionally, preliminary cross sections of the B^{5+} + H(2s) collision are also provided.

PACS numbers: 34.10.+x

1. Introduction

Charge-exchange collisional processes have acquired a great importance in the last years due to their relevancy in fusion research and astrophysics (Janev *et al* 1985, Lambert 1993, Beiersdorfer *et al* 2001). In particular, charge-exchange recombination spectroscopy (CXRS) is a basic tool in fusion plasma diagnostics (Isler 1994, Whyte *et al* 1998, Ongena 2001, Esipchuk 2003). In these experiments, a neutral beam of H or D is injected into the plasma edge, colliding afterwards with ionic impurities present in the plasma. Detailed information about the density, temperature and charge state of the impurities in different reactor regions is obtained by analyzing the radiative decay of the excited states formed by charge transfer processes. On the other hand, these collisions may often lead to excitation processes, and beam atoms in the metastable 2s state can also be found in the diagnostic beam. The use of low-Z materials such as Berylium and Boron to coat the reactor's walls instead of high-Z materials (Winter 1996), makes it usual to find B, C, O and F impurities (McCarthy *et al* 2003), that are desorbed and

progressively stripped by collisional processes as they enter inner regions of the plasma. In particular, the case of Boron is especially interesting in the TJ-II stellerator reactor (CIEMAT, Spain), as this element is employed as an enrichment for the graphite layers in device's walls. Furthermore, boronisation of the first wall of this reactor significantly improves the energy confinement of the plasma, with a lower total radiation level, a higher average neutral density and higher energy losses through charge-exchange (CX) processes (Tabarés *et al* 2003). In the TJ-II reactor, the CXRS diagnostics is undertaken in the visible spectral range, involving transitions between highly-excited states of B^{4+}. For example, the $n = 7 \rightarrow n = 6$ and $n = 8 \rightarrow n = 7$ transitions correspond to emission lines of $4946\mathring{A}$ and $7620\mathring{A}$, respectively. Therefore, since the energy of the diagnostic beam varies tipically from 15 keV/amu to 30 keV/amu, accurate n-high lying partial capture cross sections at intermediate energies are then required for the collision B^{5+}+H.

In the critical intermediate impact energy region, ionization, excitation and electron capture are competitive processes, and perturbative approaches are not applicable due to multiple scattering effects (Bransden and McDowell 1992). On the other hand, semi-classical methods have demonstrated to be suitable at these energies. In particular, the close-coupling molecular method considered here, based on an expansion of the total wavefunction over one electron diatomic molecule orbitals (OEDMs), has been successfully applied in the low/intermediate energy range for capture cross sections (see (Errea *et al* 1994, Harel *et al* 1998, Errea *et al* 1998*b*)). Moreover, it has been shown that the domain of applicability can be extended at intermediate energies assuming that the ionizing flux is implicitly described by the most excited molecular channels (Harel *et al* 1997, Errea *et al* 1998*a*, Errea *et al* 2004*a*). On the other hand, the treatment of charge transfer to very excited states implies the use of large molecular bases, which means quite cumbersome calculations. Classical methods provide an appealing alternative to overcome this limitation of the semi-classical method. In the classical trajectory MonteCarlo method (CTMC), originally developed by Abrines and Percival (1966), the separate evaluation of capture, excitation and ionization probabilities is straightforward, and the method has the advantage that capture to very energetic levels poses no problems. However, obvious limitations appear when quantal effects become significant, restricting the CTMC method to energies that are higher than the maximum of the capture cross section. Another feature that deserves attention is the generation of the initial classical electron distribution, which shall mimic the quantal initial state (Errea *et al* 2004*b*). Our previous conclusions in this respect suggest the use of two distributions (microcanonical and hydrogenic) to obtain partial capture cross sections for both low- and high-lying levels. With this double choice, it is found that the semi-classical and classical cross sections are in reasonably good agreement in the energy region around 30 keV/amu (Errea *et al* 2004*a*, Errea *et al* 2004*b*). Accordingly, a combined semi-classical and classical procedure has been used in the calculations reported here to obtain accurate partial capture cross sections for B^{5+}+H collisions. We have generated a single comprehensive cross section database, encompassing the entire low-intermediate-high energy range. The reliability of the computed cross sections is reinforced when

similar classical and quantal descriptions of the collision dynamics are obtained. This last point, partially introduced in Errea *et al* (2004*b*), has been subjected to a thorough comparative analysis, but will not be presented herein as it exceeds the scope of this paper. On the other hand, one may extend the capture databases down to very low energies by considering a similar merging between semi-classical and quantal methods (Errea *et al* 1998*b*).

Our paper is organized as follows: In section 2 we briefly introduce the three theoretical methods (quantal, semi-classical and classical) employed in this work and which were originally developed by this group (Errea *et al* 1998*b*, Errea *et al* 2004*a*). Results obtained for total and partial capture cross sections are provided in section 3, including figures and recommended datatables. Moreover, we shall focus in this section on the connection between the several methods employed. Special interest is payed to the classical method, regarding the election of the initial distribution and the continuity between ionization and capture processes, seeking for extrapolation rules at high velocities. Finally, in section 4 we draw the final conclusions, settling general considerations about the criterion employed to provide the recommended cross sections.

Atomic units are employed throughout unless otherwise stated.

2. Theoretical methods

2.1. Quantal treatment

In this formalism, the total wavefunction Ψ^J representing the collisional system is expanded for each value of the total angular momentum J in terms of molecular orbitals $\{\chi_j\}$:

$$\Psi^J(\boldsymbol{r},\boldsymbol{\xi}) = \sum_k^N \phi_k^J(\boldsymbol{\xi})\chi_k(\boldsymbol{r},\xi) \tag{1}$$

The common reaction coordinate (CRC) $\boldsymbol{\xi}$ (Mittleman 1969, Thorson and Delos 1978) is a combination of electronic ($\boldsymbol{r}$) and nuclear coordinates ($\boldsymbol{R}$):

$$\boldsymbol{\xi} = \boldsymbol{R} + \frac{1}{\mu}\boldsymbol{s}(\boldsymbol{r},R) \tag{2}$$

with

$$\boldsymbol{s} = f(\boldsymbol{r},R)\boldsymbol{r} - \frac{1}{2}f^2(\boldsymbol{r},R)\boldsymbol{R} \tag{3}$$

introduced to ensure that the truncated expansion (1) fulfills the boundary conditions (Errea *et al* 1998*b*). The switching function $f(\boldsymbol{r},t)$ is introduced to account for the electron momentum transfer problem from the target to the projectile, and corresponds to that defined in elliptical coordinates (Harel and Jouin 1990*a*, Harel and Jouin 1990*b*, Errea *et al* 1996):

$$f(\boldsymbol{r},t) = \frac{1}{2}(g_\alpha(\mu) + d) \tag{4}$$

with $d = 1 - 2p$ and

$$g_\alpha(\mu) = \alpha^{\alpha/2} \frac{\mu}{(\alpha - 1 + \mu^2)^{\alpha/2}} \tag{5}$$

In the previous expressions $\mu = (r_B - r_H)/R$ denotes the prolate spheroidal coordinate, where $\boldsymbol{r}_{B,H}$ are the electron position vectors relative to both B^{5+} and H^+ nuclei.

Substitution of the ansatz (1) in the stationary Schrödinger equation leads to a set of second order differential system for the nuclear wavefunctions $\phi_j(\boldsymbol{\xi})$. Comparison of these wavefunctions with the asymptotic Ricatti-Bessel or Coulomb functions yields the scattering matrix elements S^J_{ij}, where $\left|S^J_{ij}\right|^2$ corresponds to the $i \to j$ transition probability. The corresponding cross sections are then obtained as:

$$\sigma_{ij}(v) = \frac{\pi}{k_i^2} \sum_J (2J+1) \left|S^J_{ij} - \delta_{ij}\right|^2 \tag{6}$$

being k_i the initial momentum of the projectile.

The one-electron diatomic molecule (OEDM) orbitals (Power 1973) χ_j introduced in (1) are eigenfunctions of the fixed-nuclei Born-Oppenheimer Hamiltonian

$$H = -\frac{1}{2}\nabla^2 - \frac{Z}{r_B} - \frac{1}{r_H} \tag{7}$$

Their corresponding eigenvalues are the molecular energies of the $(B\ H)^{5+}$ system, plotted in figure 1 as functions of the internuclear distance R. When the collisional velocity is small, transitions between channels will only occur at pseudocrossings between adjacent molecular energy curves. In view of the sharp pseudocrossing at $R \approx 13$ u.a. between the $5g\sigma$ and $4f\sigma$ molecular channels, asymptotically correlated to B^{5+}+H(1s) and $B^{4+}(n = 4)$+H^+, respectively, one may expect the electron flux to be mainly transferred to the $n = 4$ capture manifold, while $4f\sigma$-$3d\sigma$ transitions are inhibited at low energies. From these reasonings, we have chosen a small molecular basis consisting of 12 OEDMs (P12) that correlates to the entrance channel and to the main $n = 4$ capture multiplet. We have verified the convergence of the cross sections with respect to increasing size of the molecular basis, for $v \leq 0.1$ a.u.

2.2. Semi-classical formalism

In this treatment we use the impact-parameter (IPM) approximation, in which the nuclear motion is described by classical straight-line trajectories with constant velocity $\boldsymbol{v}$ and impact parameter $\boldsymbol{b}$ ($\boldsymbol{R} = \boldsymbol{v}t + \boldsymbol{b}$), while the quantal description of the electronic motion is ruled by the time-dependent Schrödinger equation:

$$(H - i\partial_t|_{\boldsymbol{r}})\Psi(\boldsymbol{r}, v, b, t) = 0 \tag{8}$$

with H defined in (7). The time derivative in equation (8) is taken by keeping fixed the electron position $\boldsymbol{r}$ in the laboratory fixed frame with respect to an origin of coordinates placed at distances $p\,R$ and $q\,R$ from the target and projectile, respectively ($p + q = 1$).

In the standard molecular treatments (Errea *et al* 1994), equation (8) is solved by expanding Ψ in terms of the bound χ_k orbitals defined in the previous subsection:

$$\Psi(\boldsymbol{r},v,b,t) = e^{iU(\boldsymbol{r},t)} \sum_k a_k(v,b,t)\chi_k(\boldsymbol{r},R)e^{-i\int_0^t E_k(t')dt'} \tag{9}$$

$U(\boldsymbol{r},t) = f\boldsymbol{v}\cdot\boldsymbol{r} - f^2v^2t/2$ is a common translation factor (CTF), introduced to account for the momentum transfer problem (Schneiderman and Russek 1969, Errea *et al* 1994), and $f(\boldsymbol{r},t)$ is the same switching function as defined in (4). The connection between quantal and semi-classical methods is thus clear (Errea *et al* 1998*b*). Substitution of the ansatz (9) in Eq. (8) leads to a set of single differential equations for the expansion coefficients $a_k(v,b,t)$, which are integrated up to time t_{max}. Capture and excitation transition amplitudes $a^{A,H}_{nlm}(v,b,t\rightarrow\infty)$ are obtained by projecting at time t_{max} the total wavefunction Ψ onto the moving atomic states and using an extrapolation rule to account for the Stark effect and the residual rotation of the internuclear axis from t_{max} to infinity (Salin 1984). Finally, the cross section to a specific final (n,l,m) state is given by (Bransden and McDowell 1992):

$$\sigma^{A,H}_{nlm}(v) = 2\pi\int |a^{A,H}_{nlm}(v,b,t\rightarrow\infty)|^2 b\mathrm{d}b = 2\pi\int P_{nlm}(v,b)b\mathrm{d}b. \tag{10}$$

From the comparison of equations (10) and (6) follows the relation between quantal and semi-classical transition probabilites:

$$bP_{ij}(b) \leftrightarrow \frac{(2J+1)}{2k_i}\left|S^J_{ij}\right|^2 \tag{11}$$

that will be employed later on.

When increasing the impact velocities up to intermediate values, the adiabatic character of the pseudocrossings in figure 1 is reduced, and the number of channels effectively coupled is considerably enhanced. The avoided crossing between $4f\sigma$ and $3d\sigma$ molecular states at $R\approx 8$ a.u. now rules the collisional mechanism, and limits the distribution of the capture flux over the rest of the levels.

One feature that needs considering at these intermediate energies is the competition between capture and ionization. Within the standard molecular framework, the ionizing flux is implicitly described by the most energetic molecular channels, and thus the total capture cross section corresponds in fact to electron-loss (capture+ionization) (Harel *et al* 1997, Errea *et al* 1998*a*, Errea *et al* 2004*a*). Hence, to obtain accurate partial capture cross sections at intermediate velocities, one has to enlarge the molecular basis set by including more excited states , so that the promotion of the ionizing flux let the (lower) capture channels of interest mainly unaffected. According to this we use in our semi-classical calculations 223 OEDM orbitals (P223), asymptotically correlated to B^{5+}+H($n=1,2$) and B^{4+}($n=2-10$)+H^+, in order to obtain accurate cross sections for capture into the $n\leq 8$ levels, the higher capture shells ($n=9,10$) acting as absorbers of the ionizing flux.

2.3. The impact parameter CTMC formalism

In the classical formalism, the nuclear motion is also defined by means of straight-line trajectories ($\boldsymbol{R} = \boldsymbol{v}t + \boldsymbol{b}$), while electronic motion is described through a set of N independent trajectories $\{\boldsymbol{r}_j(t)\}$. The corresponding statistical phase-space distribution:

$$\rho(\boldsymbol{r}, \boldsymbol{p}, v, b, t) = \frac{1}{N}\sum_{j=1}^{N} \delta(\boldsymbol{r} - \boldsymbol{r}_j(t))\delta(\boldsymbol{p} - \boldsymbol{p}_j(t)) \tag{12}$$

satisfies the Liouville equation,

$$\frac{\partial \rho(\boldsymbol{r}, \boldsymbol{p}, v, b, t)}{\partial t} = -[\rho(\boldsymbol{r}, \boldsymbol{p}, v, b, t), H] \tag{13}$$

that may be considered as the classical counterpart of the time-dependent Schrödinger equation. Substitution of eq. (12) in (13) yields the well-known Hamilton equations:

$$\dot{\boldsymbol{r}}_j(t) = \frac{\partial H}{\partial \boldsymbol{p}_j(t)} \qquad \dot{\boldsymbol{p}}_j(t) = -\frac{\partial H}{\partial \boldsymbol{r}_j(t)} \tag{14}$$

that rule the temporal evolution of the N independent trajectories.

To mimic the initial H(1s) state, a standard microcanonical initial distribution (Abrines and Percival 1966) has been employed in many works with remarkable success (Olson and Salop 1977, Pascale *et al* 1990, Schultz and Krstić 1996, Errea *et al* 2004*a*), especially for the lowest n-partial capture cross sections. In such a distribution, all the electronic trajectories have initially the quantal energy -0.5 a.u.(Abrines and Percival 1966, Olson and Salop 1977), and the distribution function reads as:

$$\rho(\boldsymbol{r}, \boldsymbol{p}, v, b, t \to -\infty) = \frac{1}{8\pi^3}\delta(\frac{p^2}{2} - \frac{1}{r} + \frac{1}{2}) \tag{15}$$

This distribution exactly reproduces the quantal momentum density, but presents a too compact spatial density with a cut-off at $r = 2$ a.u.

As shown in previous references (Hardie and Olson 1983, Illescas and Riera 1999, Errea *et al* 2004*a*), significant improvement of ionization, total capture and high-n state-selective capture cross sections can be obtained using a hydrogenic initial distribution (Hardie and Olson 1983), which consists of a superposition of several microcanonical functions:

$$\rho(\boldsymbol{r}, \boldsymbol{p}, v, b, t \to -\infty) = \sum_{k=1}^{\mathcal{N}} \frac{(-2\epsilon_k)^{5/2}}{8\pi^3} a_k \delta\left(\frac{p^2}{2} - \frac{1}{r} - \epsilon_k\right) \tag{16}$$

The spatial density is in this case largely improved without scarcely damaging the momentum one (Hardie and Olson 1983). The energies ϵ_k, weights a_k and number $\mathcal{N} = 10$ of microcanonicals are chosen as explicited in ref. (Errea *et al* 2004*a*) so as to achieve good approximations to the quantal densities.

To asymptotically characterize each of the N electronic trajectories, we employ a dynamical atomic energy criterion at the end of the collision to distinguish between ionization ($\{E_H = \boldsymbol{p}^2/2 - 1/r > 0, E_B = 1/2(\boldsymbol{p} - \boldsymbol{v})^2 - Z/|\boldsymbol{r} - \boldsymbol{b} - \boldsymbol{v}t_{max}| > 0\}$), capture ($\{E_H > 0, E_B < 0\}$) and excitation ($\{E_H < 0, E_B > 0\}$) processes. Furthermore, we

obtain partial capture probabilities by employing the Becker and Mackellar binning method (Becker and MacKellar 1984). The accuracy of this method to reproduce the asymptotic bound atomic orbitals was analyzed in a previous contribution (Errea *et al* 2004*b*). The phase space is divided into exclusive subshells, each of them being associated to a single quantum state with definite n, l and m quantum numbers. The relative volume of the given subspace matches the multiplicity of the corresponding quantum shell, so that the correspondance principle is satisfied in the limit $n \to \infty$. Defining the classical counterparts for the principal and angular quantum numbers, $n_c = Z_B/\sqrt{-2E_B}$ and $l_c = |(\boldsymbol{r} - \boldsymbol{b} - \boldsymbol{v}t_{max}) \wedge (\boldsymbol{p} - \boldsymbol{v})|$, respectively, the binning method gives:

$$\left[\left(n - \frac{1}{2}\right)(n-1)n\right]^{1/3} < n_c \leq \left[n\left(n + \frac{1}{2}\right)(n+1)\right]^{1/3} \tag{17a}$$

$$l < \frac{n}{n_c}\, l_c \leq l + 1 \tag{17b}$$

$$2m - 1 < (\boldsymbol{r} \wedge \boldsymbol{p}) \cdot \boldsymbol{u}_Z \leq 2m + 1 \tag{17c}$$

Although nlm-partial capture cross sections are not obtained here, they can be obtained if required by using the previous binning for the m magnetic quantum number (eq.17c). A similiar criterion can be applied to the excitation cross sections by taking Z_H and E_H in the previous expressions.

Classical ionization P_i^C, capture $P_{c_{(n,l)}}^C$ and excitation $P_{e_{(n,l)}}^C$ probabilities

$$P_{i,c_{(n,l)},e_{(n,l)}}^C(v,b) = \int \mathrm{d}\boldsymbol{r} \int \mathrm{d}\boldsymbol{p}\rho_{i,c_{(n,l)},e_{(n,l)}}(\boldsymbol{r},\boldsymbol{p},v,b,t_{max}) \tag{18}$$

are then calculated to provide the cross sections by numerical integration over the impact parameter (10).

3. Results.

3.1. Total and partial cross sections.

In order to illustrate the accuracy of the three methods employed, total capture and ionization cross sections are displayed in figures 2(a) and (b) for the B^{5+}+H(1s) collision as a function of the impact energy. For $E \geq 70$ keV/amu, the capture classical cross sections closely agree with the results obtained by Gravielle and Miraglia (Gravielle and Miraglia 1995), Belkić *et al.* (Belkič *et al* 1992) and Das *et al.* (Das *et al* 1998) using the perturbative eikonal impulse (EI), Continuum Distorted Wave (CDW) and boundary corrected continuum intermediate state (BCCIS) methods. The first order perturbative picture of capture processes consists of a single scattering mechanism which depends on the components of the momentum distribution of the target electron that coincide with the incident velocity of the projectile (Bransden and McDowell 1992). Since the microcanonical momentum density is exact and the hydrogenic one is very close to it, both microcanonical- and hydrogenic-CTMC calculations accurately describe this mechanism and lead to similar total capture cross sections at high E. The agreement

of classical and perturbative results with the experimental data of Goffe *et al* (1979), obtained by using a crossed-beam setup and merging time-of-flight spectroscopy and coincidence techniques, is excellent at high energies. For energies below the energy range of adequacy of perturbative treatments (i.e. $E < 50$ keV/amu), the previous interpretation of the capture process is no longer valid, and the choice of the initial classical distribution becomes relevant. In this region ($10 \lesssim E \lesssim 50$ keV/amu), the accord with the results of Toshima (1994) is much better when using the hydrogenic-CTMC method, whereas the microcanonical distribution leads to an underestimation of the cross section. Such a pattern, which was already found in previous works (Errea *et al* 2004*a*, Errea *et al* 2004*b*), is even more evident when plotting the ionization cross sections (see figure 2(b)). Although the evaluation of the ionization cross section was not an aim of our work, accurate values are needed in order to establish the domain of validity of our methods, and especially of the semi-classical molecular one. We find that the excellent agreement between the hydrogenic-CTMC data and Toshima's results, and the convergence of the formers with single-centre Bessel expansion (Pons 2001) for energies above 100 keV/amu, contrasts with the low values obtained by means of the microcanonical distribution. Finally, and coming back to figure (a), we note that for low energies ($E \leq 10$ keV/amu) classical treatments show serious limitations to describe the strong adiabatic character of the pseudocrossings in the molecular framework, which become relevant at these energies. In consequence, neither the hydrogenic- nor the microcanonical-CTMC methods are able to reproduce the correct energy-shape of the capture cross section at low E.

The accuracy of our semi-classical results is highlighted by comparison to data obtained by Lüdde and Dreizler (1982) using a close-coupling method in terms of prolate spheroidal Hylleraas wavefunctions. Likewise, no significant differences appear with the results of Harel *et al* (1998), who employed a similar (but more reduced) molecular OEDM basis. This agreement confirms the convergence of both basis for describing the total capture processes. On the other hand, when focusing on the low-energy region ($E < 0.5$ keV/amu), we find considerable discrepancies with respect to the results of Fritsch and Lin (1984) by means of a two-centre atomic orbital AO+ expansion. The strong molecularization of the electronic cloud at such energies, which is hardly reproduced by a basis set restricted to the main bound channels plus a few united-atom (C^{5+}) orbitals (namely $5g\sigma$ and $4f\sigma$), could explain these discrepancies. In order to ascertain the accuracy of the semi-classical (OEDM) method employed at low energies, we have performed quantal calculations (see section 2.1) down to $E \sim 0.05$ keV/amu. Our quantal and semi-classical results are almost indistingishable down to $E \sim 0.1$ keV/amu. For lower energies, they slightly deviate from each other; this does not stem from the different sizes of the basis used in the quantal and semi-classical calculations but from the inadequacy of the IPM approximation at these extremely low impact velocities, as will be shown later. On the other hand, focusing on the higher limit of accuracy of the semi-classical method, the overlapping with the hydrogenic-CTMC curve is outstanding in the intermediate range 10 keV/amu $\lesssim E \lesssim$ 30 keV/amu. For $E \gtrsim 30$ keV/amu, the

semi-classical method provides values that are clearly overestimated. In this respect, we recall that the molecular total capture cross section corresponds in fact to electron-loss processes (ionization+capture). Accordingly, one cannot expect to obtain from the present molecular calculations the correct decreasing shape of the capture cross section in the energy domain where ionization is sizeable (see figure 2(b)).

In view of the agreement of quantal, semi-classical and classical (hydrogenic) total capture cross sections curves in the domain of validity of the methods, we have attempted to merge these curves to present 'recommended data' in table 1. The junction between semi-classical and classical results has been undertaken along the common region of accuracy of both methods ($10 \lesssim E \lesssim 30$ keV/amu); that is, where ionization is not competitive to capture and quantal effects are not important. We did not merge our semi-classical and quantal cross sections since the reliability of the semi-classical method comprises the lower velocity considered in this work ($v = 0.05$ a.u.).

The satisfactory results obtained for the total capture cross sections motivate a further merging between classical and semi-classical results for the same collision, this time regarding n and nl partial capture cross sections. Classical and semi-classical results are displayed in figure 3 as a function of the impact velocity for the $n = 4$ and $n = 7$ levels. The former corresponds to one of the most populated levels, while the latter is introduced in view of its important role in the diagnostics probes employed in fusion reactors. In the figure corresponding to $n = 4$, semi-classical results are compared to AO+ results (Fritsch and Lin 1984), showing good agreement except for velocities below 0.3 a.u. (the justification of this difference is the same as for total capture). Despite the lack of other semi-classical results for $n = 7$, the accuracy of our calculations relies on the huge molecular basis employed. With regard to perturbative results (Belkič *et al* 1992), good agreement with the classical cross section is achieved down to 1.5 a.u. for $n = 4$, which is consistent with the (empirical) validity criterion of the CDW approximation (Belkič *et al* 1992). In the $n = 7$ case, CDW results depart from classical data at $v < 2$ a.u., thus showing that the previous criterion has to be taken with care and that perturbative methods are only to be considered at high velocities.

Although the agreement between classical and semi-classical calculations is not so excellent as it was for the total cross sections, they are still in reasonably good concordance. For sake of coherence, the union between both sets of results has to be undertaken in the same velocity interval as in the total capture case (between 1.1 and 1.3 a.u., which corresponds to energies between 10 and 30 keV/am). By providing in table 2 a single partial capture database up to $n = 8$ capture levels, we satisfy one of the main objectives of this contribution. We leave for the next section the discussion of further considerations about the criteria employed in this 'combined' procedure for obtaining the recommended partial cross sections.

3.2. Continuity between capture and ionization.

We already emphasized that one of the advantages of the CTMC method is the easy computation of partial cross sections to very excited capture levels. The n^{-3} Oppenheimer extrapolation rule, which is known to be valid for high n values and high impact velocities, is commonly employed to derive such cross sections. In a previous contribution (Errea *et al* 2004*a*), we checked the accuracy of this rule by employing the CTMC method instead of the OBK (Oppenheimer 1928, Brinkman and Kramers 1930) and Born 1 methods (McDowell and Coleman 1970). Attending to the continuity between capture and ionization processes across the $E_B = 0$ threshold (E_B as defined in subsection 2.3), we may define an energy-differential cross section σ_{E_B}, where the contiuous variable E_B takes negative (capture) and positive values (ionization) across the threshold. This σ_{E_B} cross section exhibits a single maximum that moves towards higher energies when the impact velocity increases, and can be approximated in the $E_B < 0$ region to an exponential function. This finally yields the empirical expression that was explicited in (Errea *et al* 2004*a*):

$$\sigma_n^{cap} \approx K(v) Z_p^2 n^{-\beta} \exp\left[-\alpha(v) Z_p^2/2n^2\right] \tag{19}$$

where K and α are parameters to be fitted in each collision. When v and n are high enough, the exponential function in (19) approaches the unit, and the value $\beta \approx 3$ follows from considerations of continuity between the mechanisms. Fitting of the computed cross sections from $n = 1$ yields, for $v = 2.0$ a.u., $\alpha = -1.374$ a.u.$^{-1}$, $K = 7.584 \cdot 10^{-16}$ cm^2 and $\beta = 3.055$; the result is displayed in figure 4. Furthermore, it has been checked that when fitting from $n = 4$ one gets exactly the n^{-3} well-known dependance. It is noticeable that with the use of eq. (19), one can then obtain with high accuracy extrapolated values for n-partial capture cross sections, from low-lying to very high-lying levels.

3.3. B^{5+}+H(2s) collisions

Due to its interest in CXRS techniques, preliminary results for the B^{5+}+H(2s) are also included in this work. Recommended cross sections for n-partial and total capture and ionization processes, displayed in figure 5 as functions of the impact energy, were obtained by using semi-classical and classical methods. In the first case, we have employed the same basis as that of subsection 2.2, while for the CTMC calculations we have used a 'gaussian' initial distribution (Errea *et al* 2004*b*), whose specific form will be detailed in a later contribution. One of the first features to be noted is that the total capture cross section is one order of magnitude higher than for the H(1s) case. This explains why the H(2s) contribution to CXRS spectra are important even though the density of H(2s) in the plasma is lower than that of H(1s) (Isler and Olson 1988). On the other hand, the most populated levels are now capture into $n = 7$, followed by $n = 6$ and $n = 8$. This is coherent with the higher electronic energy of the corresponding entrance channel, which presents relevant pseudocrossings with those molecular states correlated

to capture $n = 7$ (see figure 1). Since our ionization absorber states, correlated to $n = 9$ and 10, lie close to the main populated channels, we have restricted our semi-classical calculations to impact energies where the ionization is negligible ($E \leq 15$ keV/amu). We then have performed a merging of the semi-classical and classical results around $6 \leq E(\text{keV/amu}) \leq 15$.

3.4. Connection between methods.

We now consider the continuity of the mechanisms obtained with the three methods in a similar way as in (Errea *et al* 2004*b*) and (Errea *et al* 1998*b*). We first focus on the lower region, and therefore consider the comparison between quantal and semi-classical methods at low velocities ($v \lesssim 0.2$ a.u.), where only a few states (those correlating to $n = 4$ capture levels) are involved in the dynamics. Both the reduced basis employed in the quantal method (P12) and the more extended one used in the semi-classical method (P223) are suitable for describing the strong adiabatic character of low-v transitions. In consequence, what we are checking with this comparison is the domain of validity of the semi-classical IPM approximation. Repulsive forces between both nuclei are not considered in this approximation, and for low velocities they may inhibit low-impact parameter nuclear trajectories. In addition, IPM does not allow energy transfer from nuclear to electronic motions, which are totally uncoupled in this framework, and this may have relevance in the dynamics at very low velocities. To get a detailed insight into the comparison of both methods, total charge transfer weighted probabilities are plotted as functions of b for the nuclear velocities $v = 0.1$ a.u. (figure 6a) and $v = 0.05$ a.u. (figure 6b). In the first case, both sets of results are in very good agreement, and exhibit the well-known Stueckelberg oscillations (Stueckelberg 1932). These oscillations arise as consequences of interferences ocurring in the neighbourhood of the avoided-crossing between the entrance channel and the $n = 4$ capture one. When reducing the impact velocity these oscillations are slightly shifted, and for low impact parameters the semi-classical curve follows a different pattern from the quantal one. The small-b peak exhibited by the former is the result of assuming the IPM approximation, where the deflection of the nuclear trajectories due to short-range interaction is not taken into account. Although this difference is restricted to very low impact parameters and thus does not affect significantly the computed cross sections, it indicates that we are reaching the lower bound of accuracy of the eikonal approximation at $v = 0.05$ a.u.

Regarding the classical / semi-classical comparison, we shall first comment that the excellent agreement observed for total capture cross sections is followed by a reasonable good comparison of the corresponding partial cross sections. In practice, such a good agreement is achieved by selecting for each capture level the most convenient initial classical distribution. Indeed, the use of a microcanonical distribution leads to a better comparison with the semi-classical results for some capture levels, while the hydrogenic distribution is preferable for some other. To understand this behaviour, we present in figure 7 the weighted probabilities for capture into $n = 3, 4, 7$ and 8, obtained for $v = 1.2$

a.u., where the semi-classical method can be considered as reference. The agreement of the microcanonical-CTMC and semi-classical probabilities is striking for $n = 3$, and remains quite good for the main populated channel $n = 4$. For higher-lying levels such as $n = 7$ and 8, this agreement severely worsens, as the microcanonical-CTMC results are clearly underestimated. In particular, these calculations do not reproduce at all the large-b probabilities, which consist of a large part of the capture processes to high n. As explained in a previous contribution (Errea *et al* 2004*b*), this liability is due to the fact that the microcanonical distribution provides a deficient description of the outer part of the spatial density (see subsection 2.3), which is involved in the long-range (i.e., large-b) inelastic transitions. Therefore, the hydrogenic initial distribution, which closely reproduces the quantal spatial density, fares better than the microcanonical one in describing the long-range transitions which tailor capture to high-lying n levels (see figure 7). In Errea *et al* (2004*b*), we showed that this improvement, achieved by selecting several initial electronic energies ϵ_k (see subsection 2.3) around the exact value -0.5 a.u., implies a considerable broadening of the initial molecular energy band. This broadening reflects in a substantial part of the electron flux falling inside very high capture levels at the end of the collision, but at the same time the lower limit of the energy band is extended in order to keep the initial average energy equal to the quantal value (-0.5 a.u.). Transitions to very low-lying levels (i.e., $n \sim 1, 2$) are then enhanced, and unitarity implies the underestimation of the probabilities for intermediate levels ($n \sim 3, 4$), as shown in figure 7. This has no correspondance with the semi-classical case where the molecular energies are quantized, which restricts the transitions to very low-lying levels even at intermediate velocities. When using the microcanonical distribution, where all the electrons have initially the exact energy, the molecular energy band is considerably narrower at the end of the collision, and the electron flux remains then focused on a few intermediate energy levels (i.e., on $n \sim 3, 4$), providing more accurate cross sections for them. Summing up, both microcanonical- and hydrogenic-CTMC calculations have to be performed to obtain a reliable description of the capture processes leading to both low- and high-lying levels.

4. Conclusions and future scopes

This work reports recommended data for total and partial (n and nl) capture cross sections for the B^{5+}+H collision in the difficult intermediate energy domain. Using a combined procedure, by means of semi-classical and classical methods, we have obtained accurate partial cross sections for highly excited states (i.e. $n = 7, 8$) of interest in fusion plasma diagnostics. One single accurate database has been built according to the following criteria:

- Semi-classical results are priorized whenever the ionization cross section is noticeably lower than the capture one ($v \leq 1.3$ a.u. and $v \leq 0.8$ a.u. for B^{5+}+H(1s) and B^{5+}+H(2s), respectively).

- The switch from semi-classical to classical results is performed on the common region of accuracy of both methods: $1.1 \leq v(\text{a.u.}) \leq 1.3$ for B^{5+}+H(1s) and $0.5 \leq v(\text{a.u.}) \leq 0.8$ for B^{5+}+H(2s).
- Regarding n- and nl-partial cross sections, the classical microcanonical distribution will be employed for the low-lying levels ($n \leq 4$) and the hydrogenic distribution for the high-lying ones ($n \geq 5$).
- Total cross sections are verified to be in excellent agreement to those obtained by adding up the corresponding partial cross sections.
- The semi-classical / classical merging of nl partial cross sections is performed attending to the normalized σ_{nl}/σ_n values. The classical initial distribution chosen for each nl level is the same as for the corresponding n level.

The semi-classical molecular close-coupling and the statistical classical MonteCarlo method, are shown to give excellent results at low-intermediate and intermediate-high energies, respectively, by comparison with other methods of proved accuracy. On the one hand, the molecular method yields capture cross sections in good agreement with atomic close-coupling results for energies below the maximum of the total capture cross section. A large molecular basis is employed so that the promotion of the ionizing flux does not pollute the partial cross sections corresponding to the desired levels. We have also checked the accuracy of this method at very low energies ($E < 1$ keV/amu) by performing also quantal CRC calculations. Slight differences appear for $E \lesssim 0.06$ keV/amu due to the inadequacy of the IPM approximation at such (very) low impact energies.

For energies where the ionization is competitive with the capture one, the use of CTMC classical method appears as an appealling alternative, due to the simplicity of its algorithms in contrast to the cited difficulties of semi-classical methods. The results obtained for high impact energies are in good agreement with perturbative results, and we have further obtained an empirical generalization of the n^{-3} extrapolation Oppenheimer rule. However, the reader should not be misled by these advantages: There are so many variants of the classical methods and the differences between them are so important (e.g., the dependency on the choice of the initial distribution) that a previous comparative study is needed until more experience is available. Nevertheless, we think that the general conclusions regarding the initial distribution obtained in this work may be extrapolated to other collisional systems. In particular, the microcanonical distribution yields an underestimation of total and high-n partial capture cross sections ($n > 4$) at intermediate energies. On the other hand, the use of a hydrogenic distribution, which reproduces fairly well the exact initial radial densities, provides a better description of the long-range transitions and therefore more accurate values of total and $n > 4$ partial capture cross sections.

Another method covering the intermediate energy domain in capture processes is the two-centre atomic close-coupling methods (Fritsch and Lin 1984, Toshima 1994, Toshima 1997, Toshima 1999), that provide total and partial capture, excitation

and ionization cross sections at the same time. However, calculations become awkward when increasing the projectile charge, or when aiming to compute high-n partial capture cross sections, since the underlying basis have to be accordingly enlarged and frequently exhibit linear dependences in the low-energy range. Since the partial capture cross sections required in our case refer to considerably high levels ($n \geq 7$), and a similar study will be needed in the next future for highly-charged collisions (e.g., $Ar^{[16,17,18]+}$) at the same intermediate energies, the required enlargement shall turn to be a serious limitation. In contrast with it, and in light of the good results achieved in this work as well as in previous contributions (Errea *et al* 2004*a*, Errea *et al* 2004*b*), the proposed 'combined' method does not reflect these limitations for highly-charged collisions, since classical methods have shown to work even better in these conditions.

ACKNOWLEDGEMENTS

The authors would like to express their thanks to Dr. F. Tabarés and Dr. K. J. McCarthy for useful data about plasma diagnostics. This work has been partially supported by DGICYT projects FIS2004-04145 and ENE2004-06266/FTN. We would like to acknowledge the Ministerio de Ciencia y Tecnología (Spain) and the Ministère des Affaires Étrangères for financial support under the coordinated program AIHF04-Picasso2004. F. G. would like to acknowledge CIEMAT for support under a resarch fellowship and J. S. would also like to acknowledge the Fundación López-Castro for its support.

References

Abrines R and Percival I. C 1966 *Proc. Phys. Soc.* **88** 861

Becker R. L and MacKellar A. D 1984 *J. Phys. B: At. Mol. Phys.* **17** 3923

Beiersdorfer P, Lisse C. M, Olson R. E, Brown G. V and Chen H 2001 *The Astrophysical Journal* **549** L147

Belkič D, Gayet R and Salin A 1992 *At. Data Nucl. Data Tables* **51** 76

Bransden B. H and McDowell M. H. C (1992) *Charge Exchange and the Theory of Ion-Atom Collisions* Oxford, Clarendon

Brinkman H. C and Kramers H. A 1930 *Proc. Acad. Sci. Amsterdam* **33** 973

Crandall D. H, Phaneuf R. A and Meyer F. W 1979 *Phys. Rev. A* **19** 504

Das M, Purkait M and Mandal C. R 1998 *Phys. Rev. A* **57** 3573

Errea L. F, Gorfinkiel J. D, Harel C, Jouin H, Macías A, Méndez L, Pons B and Riera A 1996 *Phys. Scr.* **T62** 33–38

Errea L. F, Harel C, Illescas C, Jouin H, Méndez L, Pons B and Riera A 1998*a* *J. Phys. B: At. Mol. Opt. Phys.* **31** 3199

Errea L. F, Harel C, Jouin H, Méndez L, Pons B and Riera A 1994 *J. Phys. B: At. Mol. Opt. Phys.* **27** 3603

Errea L. F, Harel C, Jouin H, Méndez L, Pons B and Riera A 1998*b* *J. Phys. B: At. Mol. Opt. Phys.* **31** 3527

Errea L. F, Illescas C, Méndez L, Pons B, Riera A and Suárez J 2004*a* *J. Phys. B: At. Mol. Opt. Phys.* **37** 4323-4338

Errea L. F, Illescas C, Méndez L, Pons B, Riera A and Suárez J 2004*b* *Phys. Rev. A* **70** 52713

Esipchuk Y. V 2003 *Plasma Phys. Control. Fusion* **45** 793

Fritsch W and Lin C. D 1984 *Phys. Rev. A* **29** 3039

Goffe T. V, Shah M. B and Gilbody H. B 1979 *J. Phys. B: At. Mol. Opt. Phys.* **12** 3763

Gravielle M. S and Miraglia J. E 1995 *Phys. Rev. A* **51** 2131

Hardie D. J. W and Olson R. E 1983 *J. Phys. B: At. Mol. Phys.* **16** 1983

Harel C and Jouin H 1990*a* *Europhys. Lett.* **11** 2121

Harel C and Jouin H 1990*b* *J. Phys. B: At. Mol. Opt. Phys.* **24** 3219

Harel C, Jouin H and Pons B 1998 *At. Data. Nucl. Data Tables* **68** 279

Harel C, Jouin H, Pons B, Errea L. F, Méndez L and Riera A 1997 *Phys. Rev. A* **55** 287

Illescas C and Riera A 1999 *Phys. Rev. A* **A60** 4546

Isler R. C 1994 *Plasma Phys. Control. Fusion* **36** 171

Isler R. C and Olson R. E 1988 *Phys. Rev. A* **37** 3399

Janev R. K, Presnyakov L. P and Shevelko V. P (1985) *Physics of Highly Charged Ions* Springer-Verlag, Heidelberg

Lambert D. L 1993 *Phys. Scr.* **T47** 186

Lüdde H. J and Dreizler R. M 1982 *J. Phys. B: At. Mol. Phys.* **15** 2713-2720

McCarthy K, Balbín R and López-Fraguas A (2003) Feasibility study on a neutral beam diagnostic injector for tj-ii Informes Técnicos Ciemat

McDowell M. R. C and Coleman J. P (1970) *Introduction to the Theory of Ion-Atom Collisions* Amsterdam, North Holland

Mittleman M. H 1969 *Phys. Rev.* **188** 231

Olson R and Salop A 1977 *Phys. Rev. A* **16** 531

Ongena J 2001 *Physics of Plasmas* **8** 2188

Oppenheimer J. R 1928 *Phys. Rev.* **31** 349

Pascale J, Olson R. E and Reinhold C 1990 *J. Phys. B: At. Mol. Opt. Phys.* **42** 5305

Pons B 2001 *Phys. Rev. A* **63** 01274

Power J. D 1973 *Phil. Soc. Trans. R. Soc* **274** 663

Salin A 1984 *J. Phys (Paris)* **45** 671

Schneiderman S. B and Russek A 1969 *Phys. Rev.* **181** 311
Schultz D. R and Krstić P. S 1996 *At. and Plasma-Material Interaction Data for Fusion* **6** 173
Sevila I (2003) PhD thesis Universidad Autónoma de Madrid
Stueckelberg E. C. G 1932 *Helv. Phys. Acta* **5** 369
Tabarés F. L, Tafalla D, Balbín R, Branas B, Estrada T, García-Cortés I, Medina F and Ochando M. A 2003 *Journal of Nucl. Mat.* **313** 839-844
Thorson W. R and Delos J. B 1978 *Phys. Rev. A* **18** 135
Toshima N 1994 *Phys. Rev. A* **50** 3940
Toshima N 1997 *Phys. Scr.* **73** 144
Toshima N 1999 *Phys. Rev. A* **59** 1981
Whyte D. G, Isler R. C, Wade M. R, Schultz D. R, Krstic P. S, Hung C. C and West W. P 1998 *Phys. Plasmas* **5** 3694
Winter J 1996 *Plasma Phys. Control. Fusion* **38** 1503

Table 1. Recommended total capture cross sections (10^{-16} cm^2) for B^{5+}+ H(1s) collision as a function of the impact velocity.

v(a.u.)	σ^{tot}	v(a.u.)	σ^{tot}
0.05	18.41	1.1	31.83
0.1	16.88	1.2	28.69
0.2	20.67	1.4	19.74
0.3	27.20	1.6	12.26
0.4	31.40	1.8	7.42
0.5	35.90	2.0	4.33
0.6	37.63	2.5	1.09
0.7	37.52	3.0	0.29
0.8	36.62	4.0	2.65(-2)
0.9	35.39	5.0	3.48(-3)
1.0	33.85	6.32	3.30(-4)

Table 2. Recommended n- and nl-state selective capture cross sections (10^{-16} cm^2) for B^{5+}+ H(1s) collision as a function of the impact velocity.

		v (a.u.)						
		0.10	0.20	0.30	0.40	0.50	0.60	0.70
n	l							
2	0	9.46(-11)	4.86(-7)	3.63(-6)	2.47(-4)	1.72(-3)	5.25(-3)	1.40(-2)
2	1	1.23(-10)	4.28(-7)	1.47(-5)	4.61(-4)	2.38(-3)	7.16(-3)	1.57(-2)
2		2.17(-10)	9.14(-7)	1.83(-5)	7.08(-4)	4.10(-3)	1.24(-2)	2.97(-2)
3	0	1.02(-2)	3.90(-1)	1.23	1.98	1.74	1.39	1.15
3	1	1.76(-2)	7.23(-1)	2.15	3.60	4.49	4.60	4.28
3	2	1.24(-2)	3.41(-1)	1.44	2.40	3.49	4.61	5.54
3		4.02(-2)	1.45	4.82	7.98	9.72	10.6	11.0
4	0	1.69	1.37	1.23	1.03	1.02	7.42(-1)	5.62(-1)
4	1	4.29	3.85	3.53	3.01	3.26	2.27	1.79
4	2	5.51	5.72	6.63	6.66	7.49	7.22	6.20
4	3	4.97	7.44	9.44	10.6	11.8	13.5	14.2
4		16.5	18.4	20.8	21.3	23.6	23.8	22.8
5	0	4.95(-2)	1.38(-1)	1.29(-1)	5.56(-2)	5.94(-2)	9.27(-2)	9.34(-2)
5	1	7.57(-2)	1.88(-1)	2.42(-1)	1.66(-1)	1.35(-1)	2.14(-1)	3.30(-1)
5	2	8.38(-2)	2.09(-1)	3.27(-1)	4.50(-1)	2.99(-1)	3.02(-1)	3.99(-1)
5	3	7.68(-2)	1.91(-1)	4.70(-1)	7.45(-1)	8.38(-1)	8.14(-1)	8.10(-1)
5	4	9.54(-2)	8.44(-2)	2.21(-1)	4.68(-1)	7.83(-1)	1.11	1.25
5		3.81(-1)	8.09(-1)	1.39	1.88	2.12	2.53	2.88
6	0	4.36(-4)	2.57(-3)	1.15(-2)	8.65(-3)	3.56(-2)	2.52(-2)	2.91(-2)
6	1	5.72(-4)	3.79(-3)	2.35(-2)	2.98(-2)	5.02(-2)	4.38(-2)	5.01(-2)
6	2	2.34(-4)	4.65(-3)	3.24(-2)	3.45(-2)	2.78(-2)	4.14(-2)	8.03(-2)
6	3	7.54(-4)	5.07(-3)	2.74(-2)	3.56(-2)	4.13(-2)	5.63(-2)	8.28(-2)
6	4	1.28(-3)	5.20(-3)	2.34(-2)	2.13(-2)	6.69(-2)	1.14(-1)	1.15(-1)
6	5	6.38(-4)	5.12(-3)	1.50(-2)	1.40(-2)	3.86(-2)	7.81(-2)	1.16(-1)
6		3.91(-3)	2.64(-2)	1.33(-1)	1.44(-1)	2.60(-1)	3.58(-1)	4.73(-1)
7	0	2.97(-5)	4.06(-4)	2.21(-3)	4.74(-3)	2.03(-2)	2.12(-2)	1.35(-2)
7	1	3.63(-5)	8.47(-4)	2.01(-3)	6.70(-3)	2.01(-2)	2.55(-2)	2.98(-2)
7	2	1.78(-5)	5.88(-4)	3.37(-3)	4.98(-3)	1.15(-2)	1.71(-2)	2.34(-2)
7	3	2.64(-5)	3.76(-4)	4.15(-3)	6.94(-3)	1.83(-2)	2.56(-2)	3.24(-2)
7	4	4.33(-5)	5.86(-4)	3.58(-3)	6.57(-3)	2.11(-2)	3.36(-2)	3.97(-2)
7	5	3.23(-5)	7.54(-4)	3.46(-3)	7.75(-3)	1.67(-2)	2.61(-2)	2.14(-2)
7	6	1.56(-5)	1.01(-3)	2.72(-3)	7.30(-3)	9.49(-3)	4.06(-2)	6.38(-2)
7		2.01(-4)	4.57(-3)	2.15(-2)	4.50(-2)	1.17(-1)	1.90(-1)	2.24(-1)
8	0	1.45(-6)	6.73(-5)	1.16(-3)	1.12(-3)	1.02(-2)	9.81(-3)	9.01(-3)
8	1	1.27(-6)	1.34(-4)	1.62(-3)	2.37(-3)	1.12(-2)	1.20(-2)	1.66(-2)
8	2	1.05(-6)	1.11(-4)	1.65(-3)	1.97(-3)	6.20(-3)	1.65(-2)	2.21(-2)
8	3	2.15(-6)	1.04(-4)	2.51(-3)	2.65(-3)	1.19(-2)	3.95(-2)	3.80(-2)
8	4	3.29(-6)	1.32(-4)	1.92(-3)	3.31(-3)	1.70(-2)	3.96(-2)	2.33(-2)
8	5	2.12(-6)	1.28(-4)	1.10(-3)	4.24(-3)	1.05(-2)	2.18(-2)	1.17(-2)
8	6	2.56(-6)	7.60(-5)	1.13(-3)	2.26(-3)	6.08(-3)	2.01(-2)	4.22(-2)
8	7	2.22(-6)	8.60(-5)	7.35(-3)	1.71(-3)	5.00(-3)	1.78(-2)	2.04(-2)
8		1.61(-5)	8.39(-4)	1.18(-2)	1.96(-2)	7.80(-2)	1.77(-1)	1.83(-1)

		v (a.u.)						
		0.80	0.90	1.00	1.10	1.20	1.40	1.60
n	l							
2	0	9 2.59(-2)	3.98(-2)	5.49(-2)	7.00(-2)	7.91(-2)	7.20(-2)	5.57(-2)
2	1	1 3.01(-2)	5.08(-2)	7.55(-2)	1.01(-1)	1.29(-1)	1.83(-1)	2.14(-1)
2		5.59(-2)	9.06(-2)	1.30(-1)	1.71(-1)	2.08(-1)	2.55(-1)	2.70(-1
3	0	1 9.97(-1)	8.65(-1)	7.34(-1)	6.08(-1)	4.92(-1)	2.35(-1)	7.84(-2)
3	1	1 3.90	3.49	3.04	2.59	2.18	1.31	6.11(-1)
3	2	1 6.03	6.03	5.68	5.13	4.52	3.61	2.26
3		10.9	10.4	9.45	8.34	7.19	5.15	2.95
4	0	1 4.75(-1)	4.33(-1)	4.05(-1)	3.80(-2)	3.42(-1)	1.59(-1)	5.23(-2)
4	1	4 1.62	1.57	1.48	1.33	1.13	7.03(-1)	3.99(-1)
4	2	5 5.14	4.18	3.38	2.76	2.26	1.61	1.10
4	3	4 13.4	11.6	9.73	8.02	6.57	3.99	2.35
4		20.6	17.8	15.0	12.5	10.3	6.45	3.90
5	0	4 1.20(-1)	1.72(-1)	2.16(-1)	2.24(-1)	1.65(-1)	4.02(-2)	3.05(-2)
5	1	7 4.43(-1)	5.05(-1)	5.33(-1)	4.97(-1)	4.22(-1)	2.49(-1)	1.79(-1)
5	2	8 6.49(-1)	8.74(-1)	9.41(-1)	8.90(-1)	8.59(-1)	5.92(-1)	4.30(-1)
5	3	7 9.80(-1)	1.27	1.50	1.56	1.51	1.03	7.17(-1)
5	4	9 1.47	1.89	2.26	2.32	2.10	1.28	6.89(-1)
5		3.66	4.71	5.46	5.53	5.04	3.19	2.04
6	0	4 4.52(-2)	5.93(-2)	7.34(-2)	7.55(-2)	6.37(-2)	2.78(-2)	1.96(-2)
6	1	5 8.82(-2)	1.80(-1)	2.45(-1)	2.69(-1)	2.79(-1)	1.89(-1)	1.19(-1)
6	2	2 1.28(-1)	2.19(-1)	3.34(-1)	4.09(-1)	4.34(-1)	3.67(-1)	2.70(-1)
6	3	7 1.15(-1)	2.72(-1)	4.49(-1)	6.17(-1)	7.12(-1)	5.91(-1)	4.22(-1)
6	4	1 1.99(-1)	3.81(-1)	6.08(-1)	7.99(-1)	8.94(-1)	6.79(-1)	4.32(-1)
6	5	6 1.97(-1)	2.77(-1)	3.40(-1)	3.91(-1)	4.14(-1)	2.96(-1)	1.59(-1)
6		8.07(-1)	1.39	2.05	2.58	2.85	2.19	1.42
7	0	2 1.67(-2)	3.10(-2)	4.74(-2)	5.67(-2)	4.70(-2)	1.86(-2)	1.36(-2)
7	1	3 4.11(-2)	7.09(-2)	1.33(-1)	2.01(-1)	1.99(-1)	1.14(-1)	8.31(-2)
7	2	1 4.83(-2)	9.28(-2)	1.79(-1)	2.86(-1)	3.14(-1)	2.34(-1)	1.81(-1)
7	3	2 6.38(-2)	1.21(-1)	2.19(-1)	3.59(-1)	4.15(-1)	3.61(-1)	2.75(-1)
7	4	4 6.66(-2)	1.33(-1)	2.48(-1)	3.94(-1)	4.71(-1)	4.12(-1)	2.73(-1)
7	5	3 8.22(-2)	1.46(-1)	1.94(-1)	2.50(-1)	2.90(-1)	2.74(-1)	1.49(-1)
7	6	1 3.74(-2)	2.74(-2)	4.45(-2)	6.70(-2)	7.33(-2)	6.04(-2)	1.30(-2)
7		3.56(-1)	6.23(-1)	1.07	1.64	1.86	1.47	9.88(-1
8	0	1 1.63(-2)	2.85(-2)	5.28(-2)	8.35(-2)	8.49(-2)	3.86(-2)	1.05(-2)
8	1	1 3.15(-2)	6.63(-2)	1.14(-1)	1.74(-1)	1.83(-1)	1.11(-1)	5.84(-2)
8	2	1 2.95(-2)	6.25(-2)	1.10(-1)	1.67(-1)	1.87(-1)	1.61(-1)	1.24(-1)
8	3	2 2.75(-2)	4.45(-2)	1.07(-1)	1.84(-1)	2.57(-1)	2.52(-1)	1.82(-1)
8	4	3 3.24(-2)	5.50(-2)	1.07(-1)	1.95(-1)	2.60(-1)	2.66(-1)	1.84(-1)
8	5	2 3.49(-2)	9.35(-2)	1.37(-1)	1.71(-1)	1.73(-1)	1.52(-1)	1.08(-1)
8	6	2 3.38(-2)	2.76(-2)	5.45(-2)	8.73(-2)	9.48(-2)	6.76(-2)	2.09(-2)
8	7	2 1.82(-2)	1.68(-2)	1.95(-2)	2.71(-2)	2.22(-2)	9.81(-4)	—
8		2.24(-1)	3.95(-1)	7.01(-1)	1.09	1.23	1.03	6.88(-1

		v (a.u.)						
		1.80	2.00	2.50	3.00	4.00	5.00	6.32
n	l							
2	0	9 4.75(-2)	3.52(-2)	1.54(-2)	5.92(-3)	8.87(-4)	1.55(-4)	1.10(-5)
2	1	1 2.08(-1)	1.89(-1)	9.05(-2)	3.67(-2)	5.85(-3)	9.01(-4)	1.44(-4)
2		2.55(-1)	2.24(-1)	1.06(-1)	4.27(-2)	6.74(-3)	1.06(-3)	1.55(-4)
3	0	1 5.13(-2)	3.52(-2)	1.38(-2)	4.91(-3)	7.01(-4)	9.21(-5)	3.48(-6)
3	1	1 3.60(-1)	2.18(-1)	7.12(-2)	2.29(-2)	3.04(-3)	4.81(-4)	6.96(-5)
3	2	1 1.40	7.77(-1)	1.88(-1)	4.57(-2)	3.42(-3)	3.42(-4)	6.96(-6)
3		1.81	1.03	2.73(-1)	7.35(-2)	7.16(-3)	9.15(-4)	8.47(-5)
4	0	1 3.36(-2)	2.49(-2)	9.70(-3)	3.39(-3)	4.23(-4)	5.53(-5)	3.68(-6)
4	1	4 2.36(-1)	1.46(-1)	4.84(-2)	1.49(-2)	1.66(-3)	2.28(-4)	1.67(-5)
4	2	5 6.51(-1)	3.91(-1)	1.06(-1)	2.65(-2)	2.06(-3)	2.34(-4)	—
4	3	4 1.36	7.17(-1)	1.12(-1)	1.67(-2)	1.53(-4)	—	—
4		2.28	1.28	2.75(-1)	6.15(-2)	4.30(-3)	5.22(-4)	2.21(-5)
5	0	4 2.17(-2)	1.51(-2)	5.92(-3)	2.58(-3)	3.18(-4)	2.98(-5)	4.29(-6)
5	1	7 1.27(-1)	8.80(-2)	3.06(-2)	1.05(-2)	1.42(-3)	2.36(-4)	2.57(-5)
5	2	8 2.89(-1)	1.97(-1)	6.04(-2)	1.86(-2)	1.81(-3)	1.54(-4)	—
5	3	7 4.39(-1)	2.72(-1)	6.40(-2)	1.21(-2)	2.72(-4)	—	—
5	4	9 3.23(-1)	1.39(-1)	1.24(-2)	5.44(-4)	—	—	—
5		1.20	7.11(-1)	1.73(-1)	4.43(-2)	3.82(-3)	4.16(-4)	2.58(-5)
6	0	4 1.35(-2)	1.04(-2)	4.13(-3)	1.40(-3)	2.32(-4)	2.60(-5)	3.33(-6)
6	1	5 8.61(-2)	5.83(-2)	2.13(-2)	6.85(-3)	8.60(-5)	1.75(-4)	1.67(-5)
6	2	2 1.82(-1)	1.25(-1)	3.92(-2)	1.15(-2)	6.46(-4)	7.87(-5)	—
6	3	7 2.69(-1)	1.66(-1)	4.26(-2)	1.04(-2)	2.01(-4)	—	—
6	4	1 2.44(-1)	1.19(-1)	1.49(-2)	8.11(-4)	—	—	—
6	5	6 5.61(-2)	1.45(-2)	7.41(-5)	—	—	—	—
6		8.51(-1)	4.94(-1)	1.22(-1)	3.10(-2)	1.94(-3)	2.78(-4)	2.21(-5)
7	0	2 9.89(-3)	7.38(-3)	2.86(-3)	1.12(-3)	1.04(-4)	1.08(-5)	—
7	1	3 5.76(-2)	3.99(-2)	1.41(-2)	4.24(-3)	5.11(-4)	7.70(-5)	6.67(-6)
7	2	1 1.25(-1)	8.54(-2)	2.51(-2)	7.67(-3)	7.01(-4)	9.21(-5)	3.33(-6)
7	3	2 1.78(-1)	1.10(-1)	2.78(-2)	5.58(-3)	1.06(-4)	—	—
7	4	4 1.60(-1)	8.24(-2)	1.29(-2)	5.80(-4)	—	—	—
7	5	3 6.41(-2)	1.72(-2)	2.85(-4)	—	—	—	—
7	6	1 1.11(-3)	3.86(-5)	—	—	—	—	—
7		5.95(-1)	3.42(-1)	8.30(-2)	1.92(-2)	1.42(-3)	1.84(-4)	1.11(-5)
8	0	1 7.74(-3)	5.08(-3)	1.86(-3)	8.64(-4)	6.73(-5)	7.69(-6)	—
8	1	1 4.29(-2)	2.72(-2)	1.01(-2)	3.15(-3)	4.36(-4)	3.92(-5)	7.50(-6)
8	2	1 8.84(-2)	6.06(-2)	1.81(-2)	6.11(-3)	4.72(-4)	5.31(-5)	2.50(-6)
8	3	2 1.25(-1)	7.75(-2)	1.98(-2)	4.63(-3)	1.24(-4)	—	—
8	4	3 1.08(-1)	5.95(-2)	7.74(-3)	6.42(-4)	—	—	—
8	5	2 5.31(-2)	1.92(-2)	2.79(-4)	—	—	—	—
8	6	2 3.11(-3)	5.83(-4)	—	—	—	—	—
8	7	2 —	—	—	—	—	—	—
8		4.27(-1)	2.50(-1)	5.79(-2)	1.54(-2)	1.11(-3)	9.58(-5)	1.47(-5)

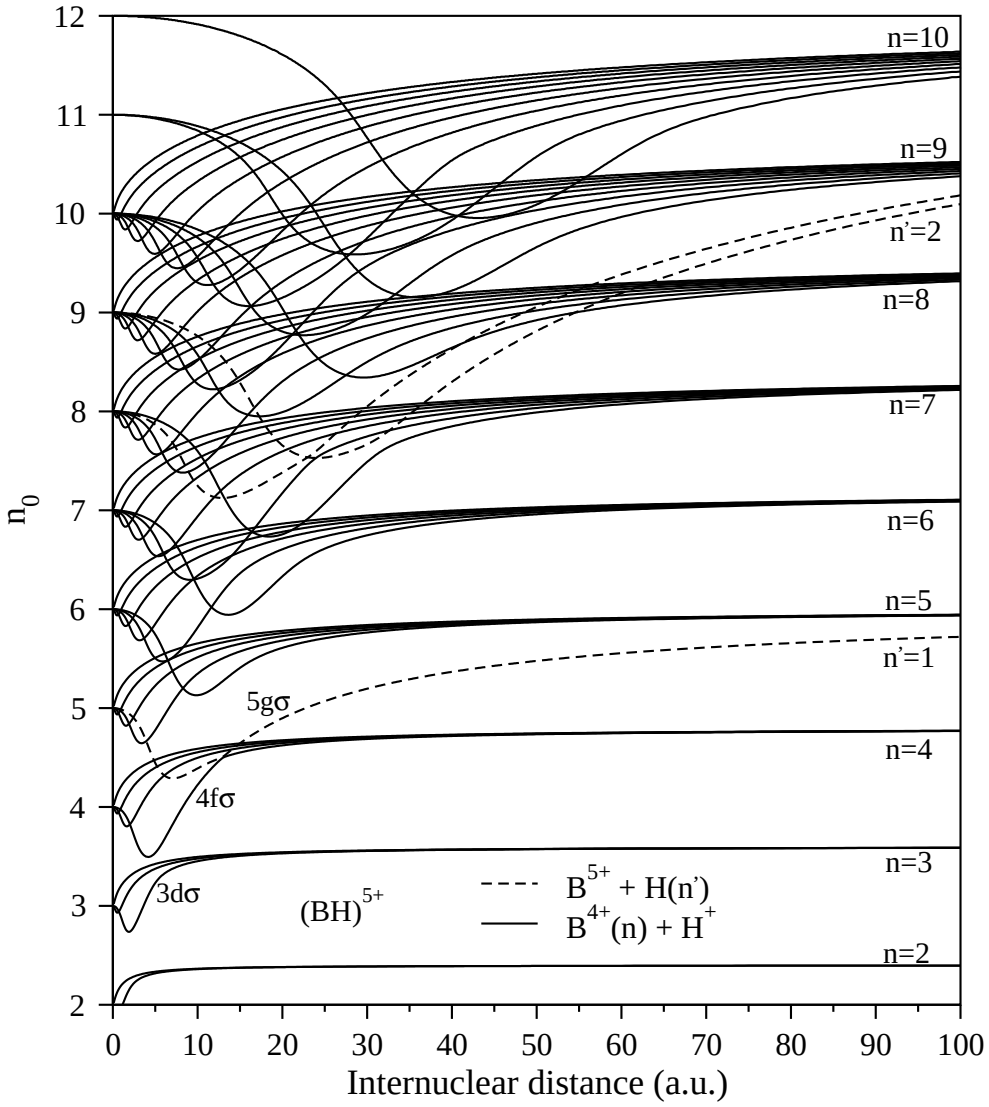

Figure 1. Energy correlation diagram for the $nl\sigma$ states of the BH^{5+} quasimolecule. Scaled energies ($n_0 = 6/\sqrt{-2\,E_{nlm=0}}$) are plotted as a function of the internuclear distance R.

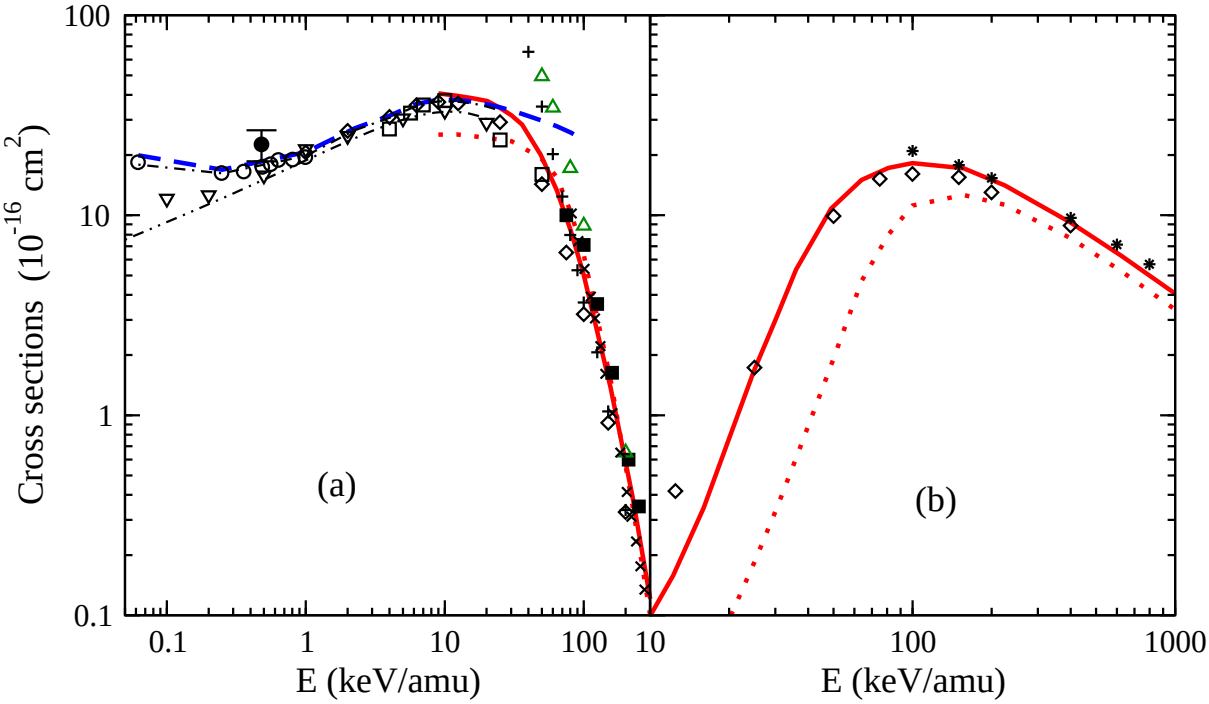

Figure 2. Total capture (1a) and ionization (1b) cross sections in B^{5+}+H(1s) collisions are displayed as a function of the impact energy E. P223 (▬ ▬ ▬) present molecular semi-classical results; present CTMC results: microcanonical (· · ·), hydrogenic (▬); present CRC results (○); experimental data for capture: (■) (Goffe *et al* 1979), (●) (Crandall *et al* 1979); other theoretical data: 2CAO (◊) (Toshima 1994), AO+ (▽) (Fritsch and Lin 1984), Hylleraas (□) (Lüdde and Dreizler 1982), P88 OEDMs (▬ · ▬) (Harel *et al* 1998), spherical Bessel (∗) (Sevila 2003) monocentric expansions; perturbative CDW (+) (Belkič *et al* 1992), EI (×) (Gravielle and Miraglia 1995) and BCCIS (△) (Das *et al* 1998) results.

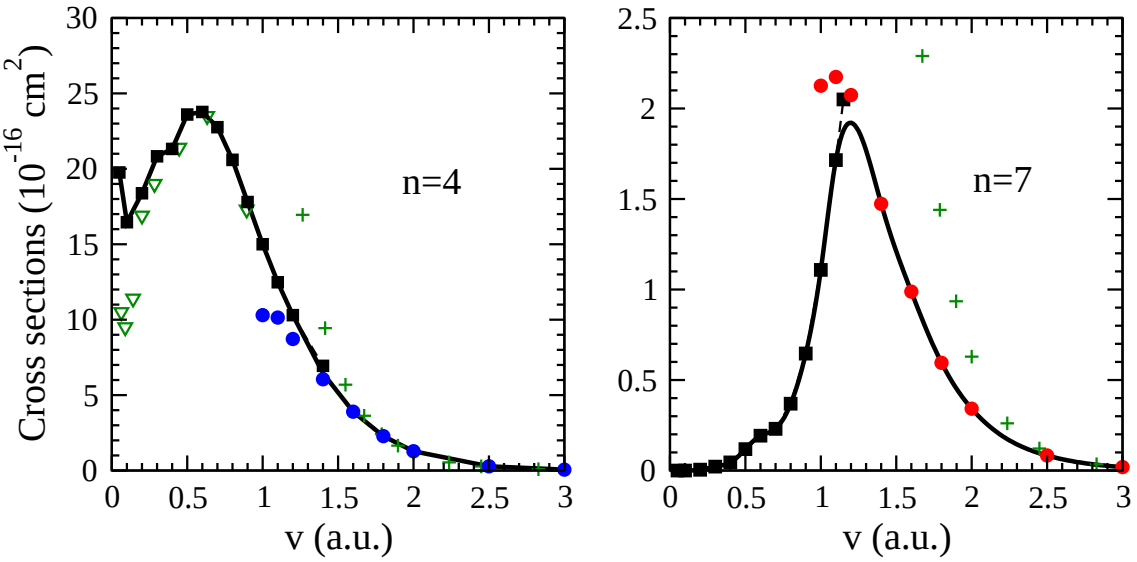

Figure 3. Single state-selective recommended cross sections as a function of the impact velocity for $n = 4$ and $n = 7$. Recommended cross sections are diplayed with a solid line, semi-classical data with solid squares and CTMC data with solid circles. Other results: perturbative CDW (+) (Belkič *et al* 1992); AO+ (▽) (Fritsch and Lin 1984).

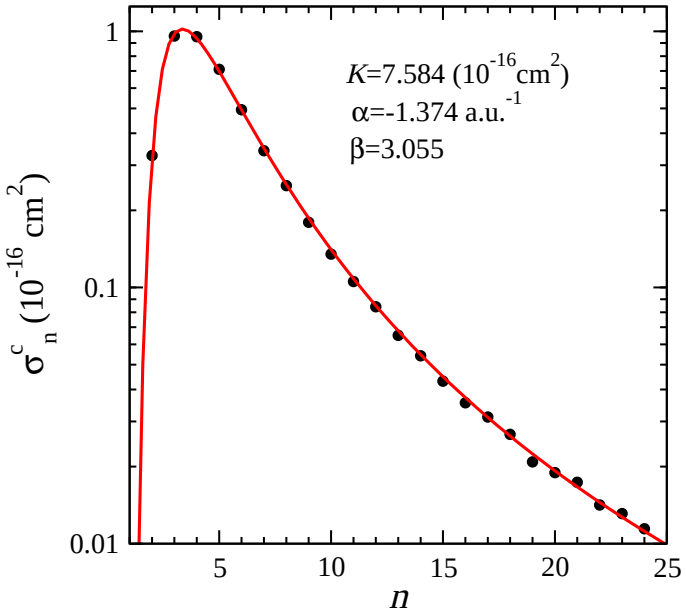

Figure 4. Illustration of the fitting (19) (solid line) obtained for the n partial cross sections (solid circles), corresponding to the hydrogenic-CTMC calculations at $v = 2.0$ a.u.

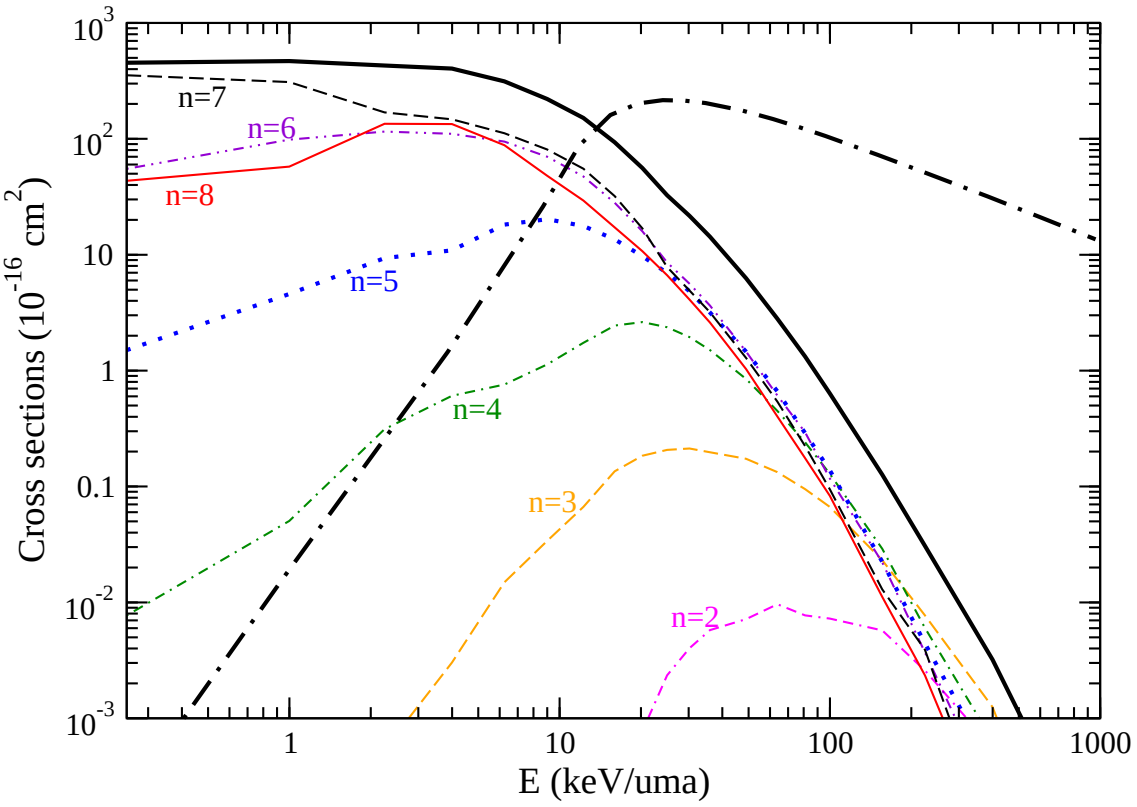

Figure 5. For the B^{5+}+H(2s) collision, total capture (——) and ionization (— · —) cross sections are plotted together with the n-partial ($n = 2-8$) capture recommended cross sections as a function of the impact energy.

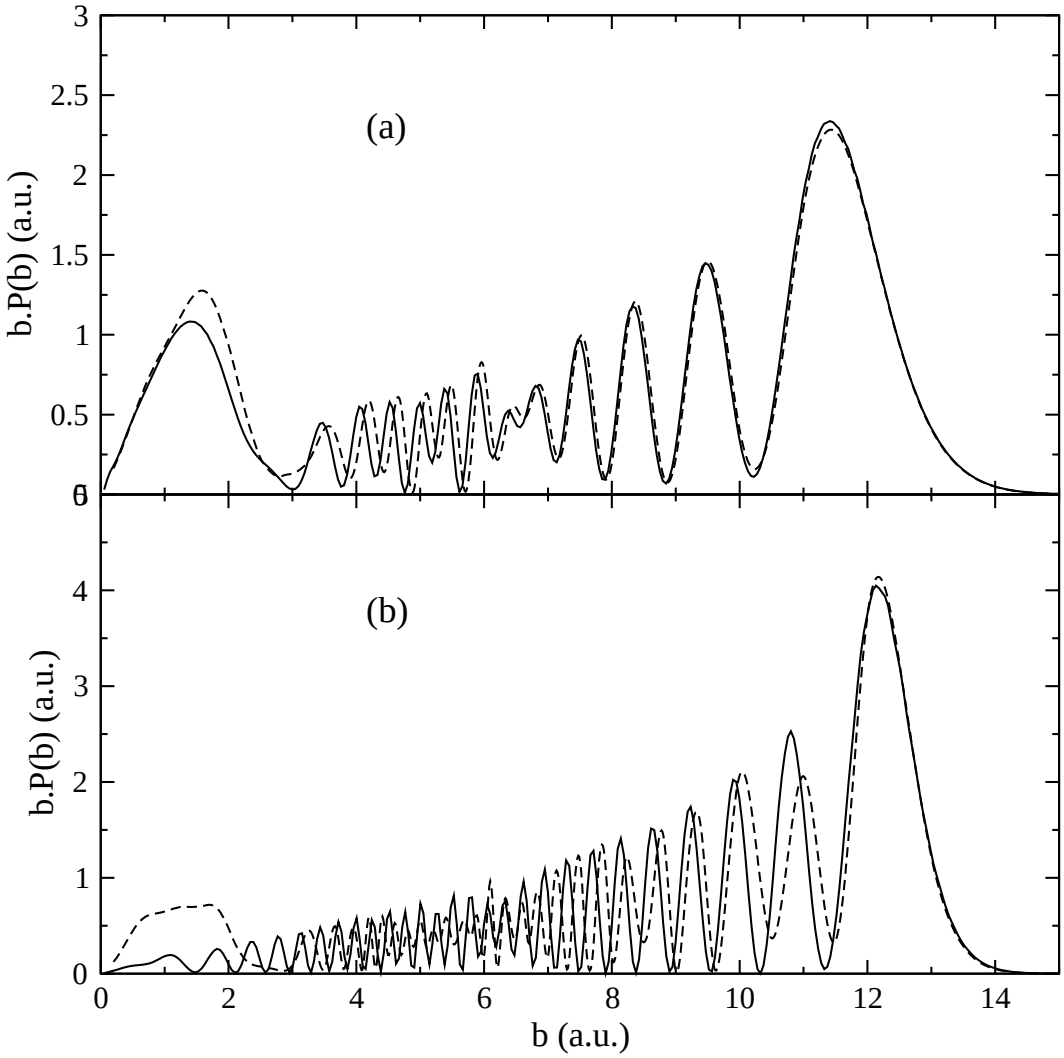

Figure 6. Comparison of the dependance of the opacity function $bP(b)$ for (a) $v = 0.1$ a.u. and (b) $v = 0.05$ a.u. with the impact parameter b for total capture molecular semi-classical (dashed line) and CRC quantal (continuous line) calculations (see eq.(11)).

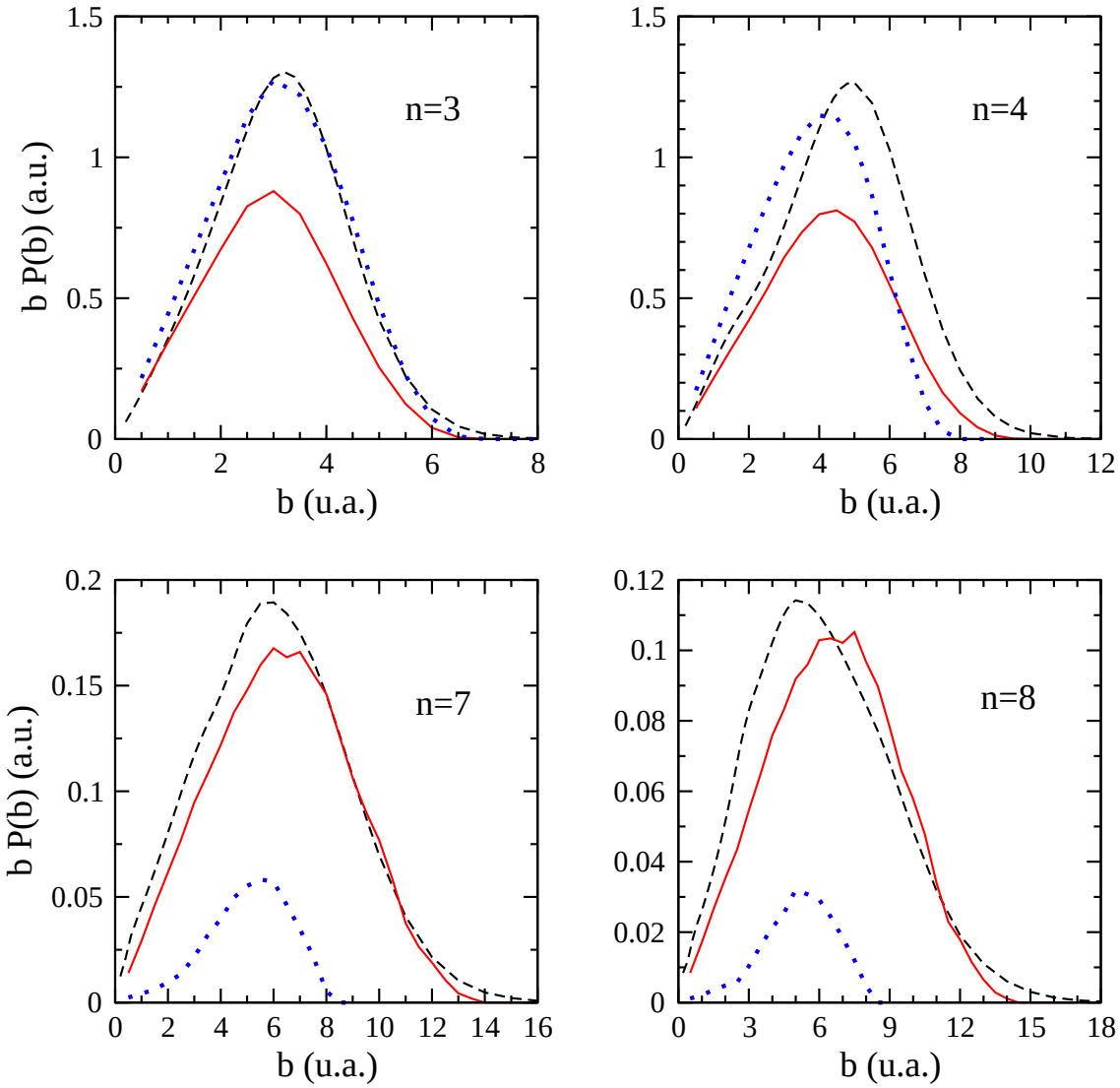

Figure 7. State-selective weighted probabilities $b\,P(b)$ as functions of the impact parameter b for capture into $n = 3, 4, 7$ and 8 at $v = 1.2$a.u.: OEDM (dashed line), CTMC-hydrogenic (solid line) and CTMC-microcanonical (dotted line).